Nanoscale

PAPER

View Article Online
View Journal

Cite this: DOI: 10.1039/c6nr00498a

Carbon phosphide monolayers with superior carrier mobility†

Gaoxue Wang,[a] Ravindra Pandey*[a] and Shashi P. Karna[b]

Received 19th January 2016,
Accepted 24th March 2016

DOI: 10.1039/c6nr00498a

www.rsc.org/nanoscale

Two dimensional (2D) materials with a finite band gap and high carrier mobility are sought after materials from both fundamental and technological perspectives. In this paper, we present the results based on the particle swarm optimization method and density functional theory which predict three geometrically different phases of the carbon phosphide (CP) monolayer consisting of sp^2 hybridized C atoms and sp^3 hybridized P atoms in hexagonal networks. Two of the phases, referred to as α-CP and β-CP with puckered or buckled surfaces are semiconducting with highly anisotropic electronic and mechanical properties. More remarkably, they have the lightest electrons and holes among the known 2D semiconductors, yielding superior carrier mobility. The γ-CP has a distorted hexagonal network and exhibits a semi-metallic behavior with Dirac cones. These theoretical findings suggest that the binary CP monolayer is a yet unexplored 2D material holding great promise for applications in high-performance electronics and optoelectronics.

Since the discovery of graphene,[1,2] two dimensional (2D) materials have sparked an extraordinary level of interest due to their unique properties and novel applications in electronics and optoelectronics. Among the 2D material family, the group IV elemental monolayers, graphene, silicene and germanene stand out due to the presence of the Dirac cones,[3,4] which endow the massless Dirac fermions with an extremely high carrier mobility. However, the gapless nature of group IV monolayers is one of the major obstacles for their applications in transistors. Recently, group V elemental monolayers such as phosphorene,[5,6] arsenene[7,8] and antimonene[9,10] were established as promising 2D materials with electronic properties which are significantly different from those of the group IV elemental monolayers. For example, phosphorene is a direct band gap semiconductor with anisotropic electronic conductance and a high hole mobility.[5,11,12] However, due to the fast degradation of phosphorene in air, its application in electronic devices has been challenging.[13–16]

Interestingly, the group IV and V elemental monolayers show noticeable structural similarities including three-fold coordinated atoms and a hexagonal network. In graphene, each C atom is sp^2 hybridized connecting to three neighboring C atoms in a planar hexagonal structure through σ bonds. The out-of-plane p_z orbitals form π and π* bands leading to its band structure with Dirac cones.[3] In phosphorene, the P atom is sp^3 hybridized sharing three of its valence electrons with neighboring P atoms forming a puckered hexagonal lattice. The remaining two valence electrons form a lone pair in one of the sp^3 orbitals. Since the preference of C and P atoms appears to be the three-fold coordination in the 2D monolayer, the following intriguing questions arise: is it possible to form a stable carbon phosphide (CP) monolayer? If yes, then how will the binary monolayer be like in terms of mechanical and electronic properties including the nature of the band gap and carrier mobility?

It is to be noted that experimental efforts are being made to produce carbon phosphide (or phosphorus carbide). Initial attempts to synthesize bulk CP were made by producing P-doped diamond-like carbon.[17] Later, the synthesis of amorphous CP films using radio frequency plasma deposition with CH_4 and PH_3 gas mixtures was reported.[18,19] The ratio of P/C in their samples can be widely controlled *via* the ratio of PH_3/CH_4 gas,[18,19] which led to the efforts of producing CP films using pulsed laser deposition[20,21] and magnetron sputtering techniques.[22] In these experiments, the presence of direct C–P

[a]*Department of Physics, Michigan Technological University, Houghton, Michigan 49931, USA. E-mail: gaoxuew@mtu.edu, pandey@mtu.edu*
[b]*US Army Research Laboratory, Weapons and Materials Research Directorate, ATTN: RDRL-WM, Aberdeen Proving Ground, MD 21005-5069, USA. E-mail: shashi.p.karna.civ@mail.mil*

†Electronic supplementary information (ESI) available: Fig. S1 cohesive energy and structure of the CP monolayer with various stoichiometric compositions obtained using CALYPSO, Fig. S2 history of CALYPSO steps and structure of the CP monolayer, Fig. S3 phonon dispersion with DFT-D2 functional, Fig. S4 band structure for β-CP using the DFT-PBE and DFT-D2 functional forms, Fig. S5 strain energy curves, Fig. S6 projected band structure for α-CP, Fig. S7 projected band structure for β-CP, Fig. S8 projected band structure for γ-CP, Fig. S9 band structures obtained with the GGA-PBE and HSE06 functional; Table S1 lattice parameters with the DFT-D2 functional form; Video S1 AIMD simulation of α-CP at 300 K, Video S2 AIMD simulation of β-CP at 300 K, Video S3 AIMD simulation of γ-CP at 300 K. See DOI: 10.1039/c6nr00498a

bonds was established. Theoretically, the properties of bulk phases of crystalline carbon phosphide with a range of stoichiometric compositions were investigated *via* density functional theory.[20,23] Various phases with three- and four-fold coordinated P atoms have been predicted.[23]

To the best of our knowledge, no experimental or theoretical study has been made on the CP monolayer. In this paper, we consider the structure, stability, mechanical and electronic properties of the low-energy phases of the CP monolayer obtained by an exhaustive structural search performed using a recently developed CALYPSO code with the particle swarm optimization method.[24]

The details of the structural search process using CALYPSO can be found in the ESI.† Fig. S1(a)† displays the low energy structures with different stoichiometric compositions of $C_{1-x}P_x$ monolayers with cohesive energies between those of graphene and phosphorene (Fig. S1(b) in the ESI†). The stable monolayers consist of three-fold coordinated C and P atoms. The stoichiometric monolayers ($x = 0.5$) have attracted our particular attention due to their compact structural configurations as shown in Fig. S2.† We classify these hexagonal configurations to be α-, β-, and γ-phases of the CP monolayer (Fig. 1) in analogy to the classification used for phosphorene, α-P (black) and β-P (blue) monolayers.[25] α-P has a puckered surface due to the intralayer sp^3 bonding character in the lattice. β-P possesses a buckled hexagonal honeycomb structure maintaining the sp^3 character of bonds. Note that the cohesive energies of α-, β-, and γ-CP are 60–90 meV per atom lower than the average cohesive energy of α-P and graphene, which implies that these structures are metastable compared to α-P and graphene. However, this does not necessarily mean that CP monolayers cannot be synthesized in experiments. For example, the layered $As_{1-x}P_x$ compounds, which are predicted to be metastable compared to layered As and layered P compounds,[26] have been synthesized.[27] Moreover, the stability of these monolayers is verified by the vibration spectra calculations and ab initio molecular dynamics (AIMD) simulations in the present study.

Calculations of electronic properties were performed using the projector-augmented-wave (PAW) method and the generalized-gradient approximation (GGA-PBE) for the electron exchange–correlation interaction[28] as implemented in the Vienna Ab initio Simulation Package (VASP).[29] The electronic and mechanical properties were obtained with the GGA-PBE functional throughout this paper. Since GGA usually underestimates the band gap, we also used the hybrid Heyd–Scuseria–Ernzerhof (HSE06) functional form[30] to get relatively accurate values of the band gap. The energy convergence was set to 10^{-6} eV and the residual force on each atom was smaller than 0.01 eV $Å^{-1}$. The energy cutoff for the plane-wave basis was set to 500 eV. The reciprocal space was sampled by *k*-point meshes of $(11 \times 11 \times 1)$ for geometry optimization, and $(45 \times 45 \times 1)$ for density of states (DOS) calculations. The vacuum distance normal to the plane was larger than 20 Å to eliminate interaction between the replicas due to the periodic boundary conditions in the supercell approach of our model. The vibration spectra calculations were performed by means of the finite displacement method as implemented in the PHONOPY program[31] with a supercell size of $(3 \times 4 \times 1)$, $(8 \times 5 \times 1)$, and $(4 \times 5 \times 1)$ for α-, β-, and γ-CP, respectively. The AIMD simulations were based on the NVT ensemble with a time step of 1 fs. The temperature was controlled to 300 K with a Nośe–Hoover thermostat.[32] In this work, the van der Waals (vdW) term was also included as in the DFT-D2 method of Grimme[33] to check the structure, stability and electronic properties of α-, β-, and γ-CP. Consistent results were obtained with GGA-PBE and DFT-D2 functional forms as shown in Fig. S3, S4 and Table S1.†

In α-, β-, and γ-CP, each C atom bonds with the three nearest neighbors in a planar configuration (see the side views in Fig. 1) implying that the C atoms are sp^2 hybridized. On the other hand, each P atom bonds with three neighboring atoms in a buckled configuration suggesting sp^3 hybridization of P atoms in the 2D lattice. For α- and β-CP, the zigzag (*i.e.* *y*) direction is composed of alternating C and P atoms, and the armchair (*i.e.* *x*) direction is composed of alternating C–C and

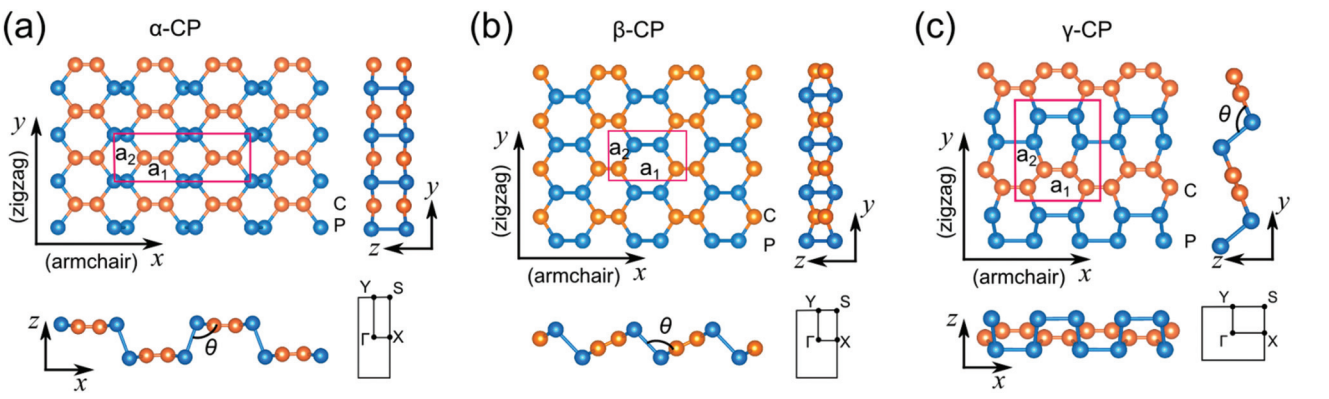

Fig. 1 The structural geometry including top view, side view, and the Brillouin zone of (a) α-CP, (b) β-CP, and (c) γ-CP. a_1 and a_2 are the lattice constants, *R* is the nearest neighbor distance, θ is the bond angle of C–P–P.

Table 1 Calculated structural parameters of CP monolayers (see Fig. 1) at the GGA-PBE level of theory

	a_1 (Å)	a_2 (Å)	R_{C-C} (Å)	R_{C-P} (Å)	R_{P-P} (Å)	θ (°)	Cohesive energy (eV per atom)
α-CP	8.68	2.92	1.36	1.83	2.32	97.40	5.32
β-CP	4.72	2.91	1.37	1.82	2.33	97.78	5.33
γ-CP	4.80	5.63	1.45, 1.43	1.82	2.30, 2.17	104.00	5.35

P–P dimers. Overall, α-CP has a puckered surface, and β-CP has a buckled surface as seen from the side views in Fig. 1(a) and (b). γ-CP is composed of alternating P chains and C chains along the armchair direction (Fig. 1(c)). Due to a mismatch in C–C and P–P bonds, γ-CP has a distorted hexagonal network.

All three phases of the CP monolayer have nearly degenerate cohesive energy with the rectangular unit cells as summarized in Table 1. The length of the C–C, C–P, and P–P bonds in α- and β-CP are 1.36–1.37 Å, 1.82–1.83 Å, and 2.32–2.22 Å, respectively. The C–C bond in the CP monolayer is slightly shorter than that of 1.42 Å in graphene,[3] and the P–P bond is slightly longer than that of 2.26 (2.22) Å in phosphorene calculated at the same level of theory.[5] In γ-CP, the length of C–C and P–P bonds varies in the range 1.43–1.45 Å and 2.17–2.30 Å, respectively which are very close to those of graphene and phosphorene. Typical C–P bond lengths of 1.85 Å were reported in the bulk CP by GGA-PBE calculations.[23]

The phonon dispersion curves are displayed in Fig. 2 showing no imaginary (negative) vibration mode in the Brillouin zone. AIMD simulations (Videos S1–S3 in the ESI†) show that α-, β-, and γ-CP maintain their structural integrity up to 5 ps demonstrating the dynamical stability of α-, β-, and γ-CP. It is to be noticed that the slopes of the longitudinal acoustic (LA) branch along Γ–X are significantly different from those along Γ–Y near Γ. The speed of sound derived from the LA branch along Γ–X (armchair) and Γ–Y (zigzag) directions is found to be (5.9, 12.0 km s^{-1}), (6.3, 12.3 km s^{-1}), and (13.3, 6.8 km s^{-1}) for α-, β-, and γ-CP, respectively, reflecting the anisotropic nature of the in-plane stiffness. The maximum vibrational frequency at 1450 cm^{-1} for the optical branches of α-, and β-CP is associated with C atoms as seen in the phonon density of states affirming a high strength of C–C bonds. Additional calculations based on the strain energy curves[34,35] (Fig. S5 in the ESI†) reveal the in-plane stiffness along the armchair and zigzag directions to be (18.8, 171.5 N m^{-1}), (46.6, 158.3 N m^{-1}), and (233.2, 51.9 N m^{-1}) for α-, β-, and γ-CP, respectively confirming the anisotropy nature of the mechanical properties. The lower stiffness along the armchair direction is due to the puckered or buckled nature of the α- and β-CP lattice (Fig. 1(a) and (b)) which could accommodate external strains by changing the puckered or buckled angle without much distortion of the bond length. This is similar to the anisotropic mechanical properties observed for phosphorene.[36,37] For γ-CP, the stiffness along the armchair direction is larger than the value in the zigzag direction because of the C chains. The in-plane stiffness of CP monolayers is smaller than that of 340 N m^{-1} in graphene,[34,38] while it is larger than that of 28.9 N m^{-1} and 101.6 N m^{-1} in phosphorene[39] (except for α-CP along the armchair direction) due to the existence of stronger C–C and C–P bonds with sp^2 hybridization in the hexagonal lattice.

The electronic properties of the α-CP monolayer are presented in Fig. 3. The calculated band structure and density of states (DOS) indicate the α-CP monolayer to be a semiconductor with an indirect band gap of 0.63 eV at the GGA-PBE level of theory. The valence band maximum (VBM) is at Γ with a value of −4.05 eV. The conduction band minimum (CBM) is located at Y with a value of −3.42 eV. The direct energy gap at Γ is 40 meV larger than the indirect gap from Γ to S. The C-p_z and P-p_z orbitals dominate the VBM and the CBM as seen in the decomposed band structure in Fig. S6.†

The band structure and DOS indicate the β-CP monolayer to be a semiconductor with a band gap of 0.39 eV (Fig. 4(a)). CBM is at X with a value of −3.76 eV, and VBM at −4.15 eV lies very close to X. Since the energy of the first VB at the X point is only 10 meV lower than VBM, we may identify the gap to be a quasi-direct band gap for the β-CP monolayer. The C-p_z and P-p_z orbitals dominate VBM, and C-p_z and P-p_x orbitals mainly contribute to CBM as seen in the decomposed band structure in Fig. S7.† Bader charge analyses reveal a similar

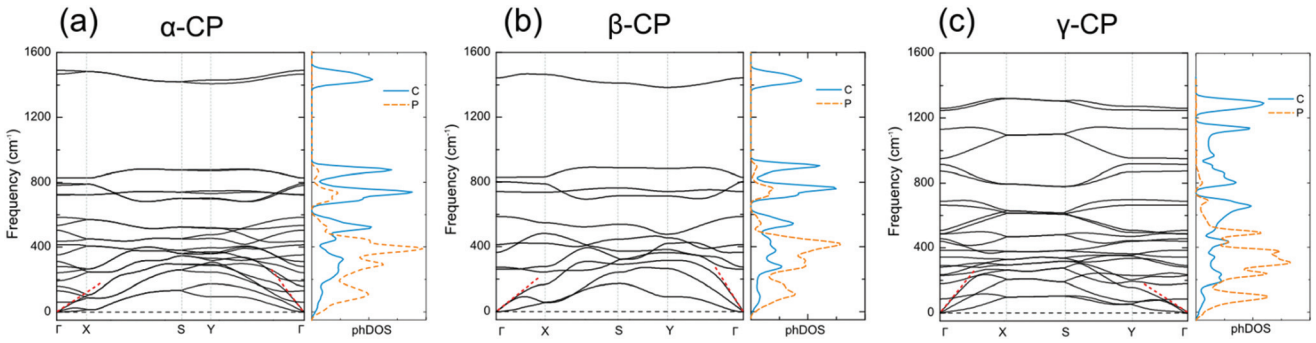

Fig. 2 The phonon dispersion and phonon density of states (phDOS) calculated for (a) α-CP, (b) β-CP, and (c) γ-CP.

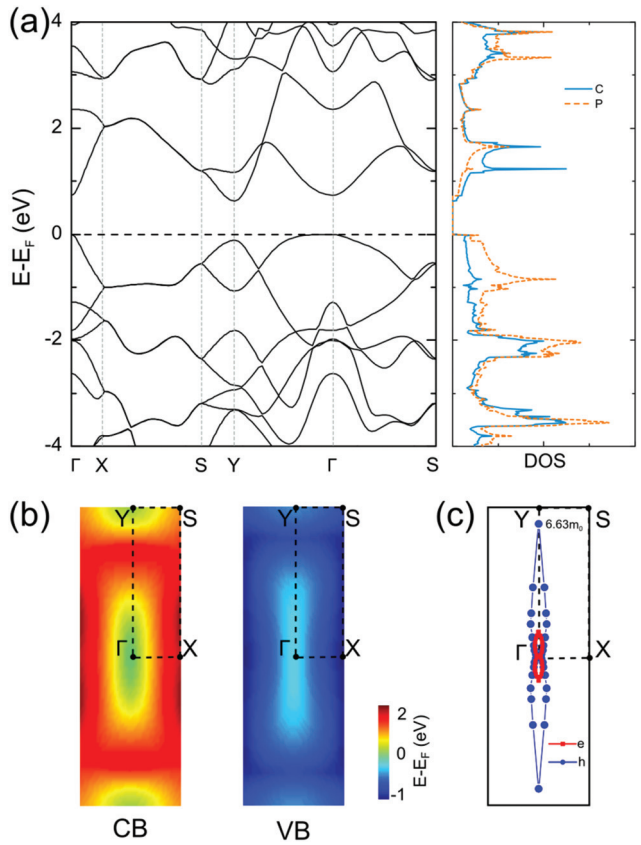

Fig. 3 Electronic properties of α-CP: (a) band structure and density of states, the inset is the zoomed figure around the V point, (b) 2D energy profiles of the first valence band (VB) and the first conduction band (CB), and (c) effective mass of electrons and holes at Γ along different directions; distance from a data point to Γ is proportional to the magnitude of the effective mass. The solid line acts as a guide to the eye.

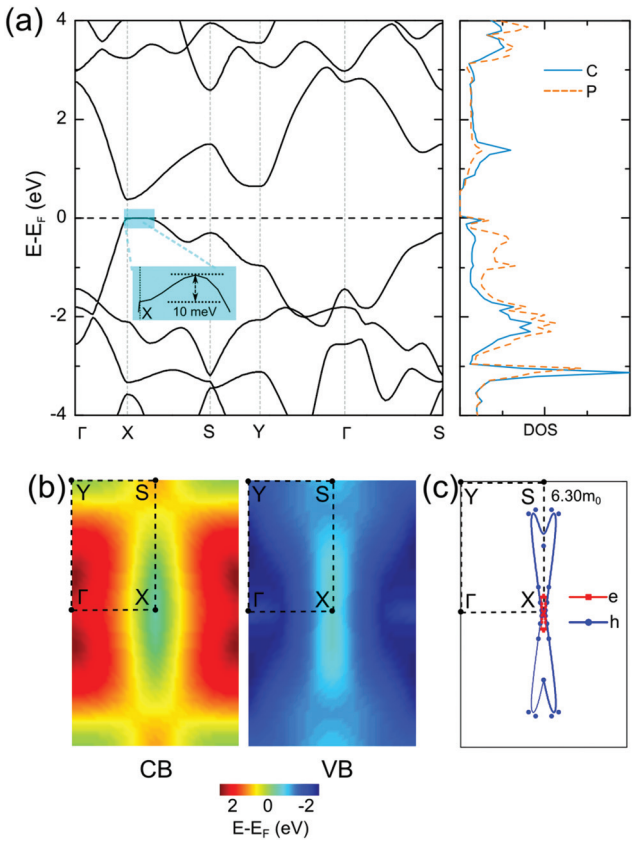

Fig. 4 Electronic properties of the β-CP monolayer: (a) band structure and density of states, (b) 2D energy dispersion of the first valence band (VB) and the first conduction band (CB), and (c) effective mass of electrons and holes along different directions at X; distance from a data point to X is proportional to the magnitude of the effective mass. The solid line acts as a guide to the eye.

charge transfer of 0.92e and 0.99e from the P atom to the C atom in α- and β-CP, respectively.

The α- and β-CP monolayers are found to show a high anisotropy in their electronic properties. For example, the valence and conduction bands around the Fermi level have different slopes along the X–Γ (armchair) and X–S (zigzag) directions (Fig. 4(a)), which reflects the directional dependence of the effective mass of electrons and holes in β-CP. From the 2D plots of the energy dispersion of the first valence and conduction bands shown in Fig. 4(b), we see an elongated shape along X–S. In contrast, the bands encounter a higher degree of dispersion along X–Γ reflecting a smaller effective mass of carriers.

The calculated directional dependence of the effective mass of carriers is shown in Fig. 4(c). The values are significantly larger in the X–S (zigzag) direction than in the X–Γ (armchair) direction. Along the X–Γ (armchair) direction, electrons and holes have effective masses smaller than 0.05m_0. The values along the X–S (zigzag) direction are 1.10m_0 and 4.10m_0, respectively. The effective mass of holes could reach a maximum of 6.30m_0 near the X–S direction. α-CP also has a significant anisotropic effective mass as demonstrated in Fig. 2(a)–(c).

The effective masses of carries in α- and β-CP along the zigzag (y) direction are comparable to the values in phosphorene (1.12m_0 and 6.35m_0 in ref.12,39,40), while the values along the armchair (x) direction are even smaller than those in phosphorene (0.17m_0 and 0.15m_0 [39,40]). The decomposed band structures in Fig. S6 and S7† reveal that the heavier holes along the zigzag direction (the first VB along Γ–Y and X–S directions in Fig. S6 and S7,† respectively) are mostly contributed by the P-p$_z$ orbital, and the lighter holes along the armchair direction (the first VB along Γ–X direction in Fig. S6 and S7†) are mainly associated with C-p$_z$ and P-p$_z$ orbitals. Therefore, contributions of C-p$_z$ electrons appear to decrease the effective mass of carriers in the binary carbon phosphide monolayer which are extremely important for nanoscale devices requiring semiconducting materials with a high carrier mobility.

An understanding of the electronic conductance of the material can be gained from the carrier mobility calculations based on the deformation potential (DP) theory as proposed by

Bardeen and Shockley.[41] According to the DP theory, the carrier mobility of 2D materials can be evaluated according to the following expression[12,39,42]

$$\mu_x = \frac{eh^3 C_x}{(2\pi)^3 k_B T m_x^* m_d (E_{1x}^2)} \quad (1)$$

where e is the electron charge, h is the Planck's constant, T is the temperature and m^* is the effective mass. m_d is determined by $m_d = (m_x^* m_y^*)^{1/2}$. E_{1x} is the deformation potential defined as $E_{1x} = \Delta V/(\Delta a_x/a_x)$, and is obtained by varying the lattice constant a_x along the direction of electron conduction. ΔV is the change in the band energy. The in-plane stiffness constant C_x is obtained by evaluating the strain energy curve.[34,35] Eqn (1) was demonstrated previously to give a reliable estimate for the upper limit of the carrier mobility in phosphorene.[12,39]

The calculated carrier mobility using eqn (1) at room temperature (T = 300 K) for α- and β-CP is summarized in Tables 2 and 3, respectively. The carrier mobility shows a strongly directional dependence as one would expect from the anisotropic nature of the calculated effective masses for α- and β-CP. The electron and hole mobility along the armchair direction is significantly larger than those obtained along the zigzag direction suggesting the presence of an anisotropic conductance in α- and β-CP. Such a strong anisotropy in carrier mobility can be measured in experiments[5] and may facilitate the fabrication of anisotropic electronic devices. More interesting than the anisotropic electronic conductance is the large value of the carrier mobility in CP monolayers. For example, the hole mobility at room temperature in α-CP could potentially reach 1.15 × 10^5 cm^2 V^{-1} s^{-1}, which is approximately five times larger than the maximum value in phosphorene (0.26 × 10^5 cm^2 V^{-1} s^{-1} (ref. 35)), and significantly larger than other 2D materials, such as MoS_2.[43] Such a large hole mobility in α-CP is attributed to a small effective mass together with a small deformation potential along the armchair direction (Table 2). β-CP has comparable hole mobility to phosphorene, while the electron mobility is much larger than in phosphorene.[35]

Distinct from α- and β-CP, γ-CP is found to be a semimetal as shown in Fig. 5. From the band structure in Fig. 5(a), it can be seen that VB and CB cross at the V point on Γ–X. The 2D and 3D energy dispersion plots in Fig. 5(b) and (c) illustrate that VB and CB touch at V and V′ in the Brillouin zone forming distorted Dirac cones. An average of 0.46e is transferred from the P atom to C atom from Bader charge analysis. The decomposed band structure in Fig. S8† demonstrates that overlapping of C-p_z and P-p_z orbitals is responsible for the emergence of Dirac cones. Calculations with a step size of 0.0013 $Å^{-1}$ along Γ–X were performed to calculate the Fermi velocity $\left(v_k = \left(\frac{1}{\hbar}\right)\left(\frac{\partial E_k}{\partial k}\right)\Big|_{E_k=E_F}\right)$. The calculated ν_F values for electrons and holes along the V–X direction are 0.78 × 10^6 m s^{-1} and 0.40 × 10^6 m s^{-1}, respectively. The Fermi velocity of electrons is close to the value in graphene (v_F = 0.85 × 10^6 m s^{-1} (ref. 44)) implying the high electron mobility in γ-CP.

The band structures of α-, β-, and γ-CP based on the hybrid HSE06 functional are shown in Fig. S9.† A relatively large band gap of 1.26 eV (0.87 eV) is obtained for α-CP (β-CP). Note that the hybrid HSE06 functional finds nearly the same shape of the band structure as is obtained by the GGA-PBE functional form. The semi-metallic properties of γ-CP are also verified with the HSE06 functional form. Therefore, γ-CP is like graphyne showing Dirac fermions in a rectangular lattice.[34,45]

The most appealing properties which make carbon phosphide monolayers intriguing members of the 2D material family are the anisotropic nature of electronic conductance and high carrier mobility. α- and β-CP monolayers are predicted to have strongly anisotropic electronic properties together with the smallest effective mass of carriers (≈0.10m_0, and 0.05m_0, respectively) among the known 2D semiconductors such as phosphorene (0.15m_0)[39,40] and MoS_2 (0.45m_0).[46]

α-, β-, and γ-CP monolayers cannot be fabricated with the mechanical exfoliation methods due to the absence of layered bulk counterparts. The possible synthesis approach can be chemical vapor deposition (CVD) which has been successfully

Table 2 Calculated carrier mobility in the α-CP monolayer at T = 300 K along the x (armchair) and y (zigzag) directions obtained at the GGA-PBE level of theory. m_e^* and m_h^* are the effective masses of electrons (e) and holes (h), respectively

	m_e^*/m_0	m_e^*/m_0	E_{1x}	E_{1y}	C_x	C_y	μ_x	μ_y
	x	y	(eV)		(N m^{-1})		(10^3 cm^2 V^{-1} s^{-1})	
e	0.10	1.22	1.72	10.55	18.75	171.47	3.87	0.08
h	0.12	6.63	0.18	1.75	18.75	171.47	115.18	0.20

Table 3 Calculated carrier mobility in the β-CP monolayer at T = 300 K along the x (armchair) and y (zigzag) directions obtained at the GGA-PBE level of theory. m_e^* and m_h^* are the effective masses of electrons (e) and holes (h), respectively

	m_e^*/m_0	m_e^*/m_0	E_{1x}	E_{1y}	C_x	C_y	μ_x	μ_y
	x	y	(eV)		(N m^{-1})		(10^3 cm^2 V^{-1} s^{-1})	
e	0.05	1.10	2.56	9.30	46.56	158.27	12.91	0.15
h	0.05	4.10	1.68	1.66	46.56	158.27	15.52	0.66

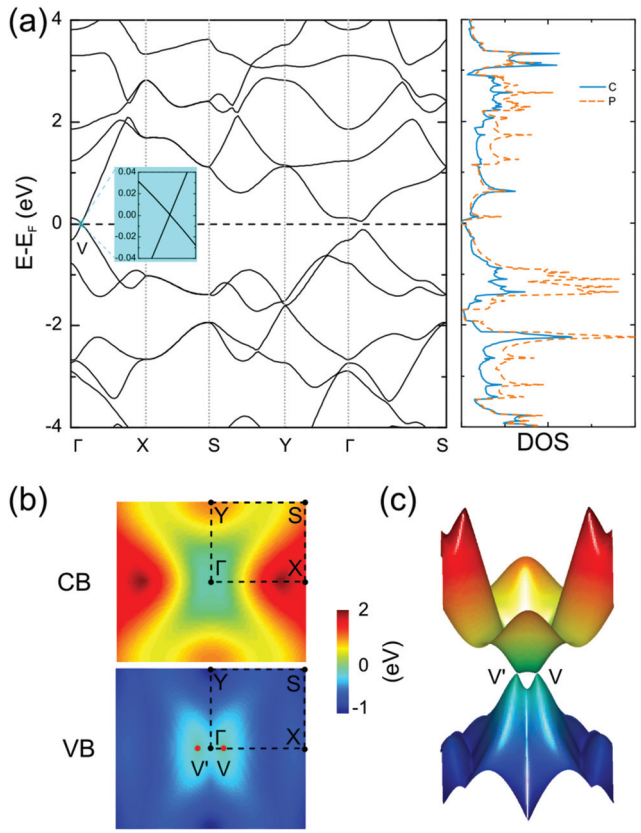

Fig. 5 Electronic properties of the γ-CP monolayer: (a) band structure and density of states, (b) 2D energy dispersion of the first CB and first VB, and (c) 3D plot for the first VB and first CB. V and V′ are the Dirac points in the Brillouin zone.

used to synthesize 2D materials including group IV monolayers, such as graphene[47,48] and silicene,[49,50] and group V thin films, such as Bi(111) and Bi(110).[51,52] We also notice recent progress in the fabrication of carbon phosphide thin films including strong evidence of the formation of C–P bonded regions in samples prepared with the pulsed laser deposition method;[21] the black phosphorus–graphite composites with sp^2 hybridized P–C bonds using the mechanical milling process have also been reported.[53] The present work will further inspire the experimental realization of CP monolayers.

In summary, the structure, stability and electronic properties of CP monolayers, namely α-, β-, and γ-CP, have been predicted. The structural configurations are comprised of sp^2 hybridized C and sp^3 hybridized P atoms in hexagonal networks. α- and β-CP are semiconductors with a high anisotropy in electronic and mechanical properties. A large carrier mobility is predicted due to the small effective mass of the carriers. γ-CP is semi-metallic with Dirac cones. Our results suggest that the yet unexplored binary carbon phosphide monolayers hold great promise for applications in high-performance electronics and optoelectronics at the nanoscale.

Acknowledgements

RAMA and Superior high performance computing clusters at Michigan Technological University were used to obtain results presented in this paper. Support from Dr S. Gowtham is gratefully acknowledged. This research was partially supported by the Army Research Office through grant number W911NF-14-2-0088.

References

1 K. S. Novoselov, A. K. Geim, S. Morozov, D. Jiang, Y. Zhang, S. A. Dubonos, I. Grigorieva and A. Firsov, *Science*, 2004, **306**, 666–669.
2 A. K. Geim and K. S. Novoselov, *Nat. Mater.*, 2007, **6**, 183–191.
3 A. C. Neto, F. Guinea, N. Peres, K. S. Novoselov and A. K. Geim, *Rev. Mod. Phys.*, 2009, **81**, 109.
4 S. Cahangirov, M. Topsakal, E. Aktürk, H. Şahin and S. Ciraci, *Phys. Rev. Lett.*, 2009, **102**, 236804.
5 H. Liu, A. T. Neal, Z. Zhu, Z. Luo, X. Xu, D. Tománek and P. D. Ye, *ACS Nano*, 2014, **8**, 4033–4041.
6 L. Li, Y. Yu, G. J. Ye, Q. Ge, X. Ou, H. Wu, D. Feng, X. H. Chen and Y. Zhang, *Nat. Nanotechnol.*, 2014, **9**, 372–377.
7 C. Kamal and M. Ezawa, *Phys. Rev. B: Condens. Matter*, 2015, **91**, 085423.
8 Z. Zhang, J. Xie, D. Yang, Y. Wang, M. Si and D. Xue, *Appl. Phys. Express*, 2015, **8**, 055201.
9 S. Zhang, Z. Yan, Y. Li, Z. Chen and H. Zeng, *Angew. Chem., Int. Ed.*, 2015, **127**, 3155–3158.
10 G. Wang, R. Pandey and S. P. Karna, *ACS Appl. Mater. Interfaces*, 2015, **7**, 11490–11496.
11 V. Tran, R. Soklaski, Y. Liang and L. Yang, *Phys. Rev. B: Condens. Matter*, 2014, **89**, 235319.
12 R. Fei and L. Yang, *Nano Lett.*, 2014, **14**, 2884–2889.
13 A. Favron, E. Gaufrès, F. Fossard, A.-L. Phaneuf-L'Heureux, N. Y. Tang, P. L. Lévesque, A. Loiseau, R. Leonelli, S. Francoeur and R. Martel, *Nat. Mater.*, 2015, **14**, 826–832.
14 J. O. Island, G. A. Steele, H. S. van der Zant and A. Castellanos-Gomez, *2D Mater.*, 2015, **2**, 011002.
15 G. Wang, W. J. Slough, R. Pandey and S. P. Karna, 2015, arXiv preprint arXiv:1508.07461, accepted by 2D Materials.
16 G. Wang, R. Pandey and S. P. Karna, *Nanoscale*, 2015, **7**, 524–531.
17 D. Jones and A. Stewart, *Philos. Mag. B*, 1982, **46**, 423–434.
18 M. Kuo, P. May, A. Gunn, M. Ashfold and R. Wild, *Diamond Relat. Mater.*, 2000, **9**, 1222–1227.
19 S. Pearce, P. May, R. Wild, K. Hallam and P. Heard, *Diamond Relat. Mater.*, 2002, **11**, 1041–1046.
20 F. Claeyssens, G. Fuge, N. Allan, P. May and M. Ashfold, *Dalton Trans.*, 2004, 3085–3092.
21 J. N. Hart, P. W. May, N. L. Allan, K. R. Hallam, F. Claeyssens, G. M. Fuge, M. Ruda and P. J. Heard, *J. Solid State Chem.*, 2013, **198**, 466–474.

22 A. Furlan, G. K. Gueorguiev, Z. Czigány, H. Högberg, S. Braun, S. Stafström and L. Hultman, *Phys. Status Solidi*, 2008, **2**, 191–193.
23 F. Claeyssens, J. N. Hart, N. L. Allan and J. M. Oliva, *Phys. Rev. B: Condens. Matter*, 2009, **79**, 134115.
24 Y. Wang, J. Lv, L. Zhu and Y. Ma, *Phys. Rev. B: Condens. Matter*, 2010, **82**, 094116.
25 Z. Zhu and D. Tománek, *Phys. Rev. Lett.*, 2014, **112**, 176802.
26 Z. Zhu, J. Guan and D. Tománek, *Nano Lett.*, 2015, **15**, 6042–6046.
27 B. Liu, M. Köpf, A. N. Abbas, X. Wang, Q. Guo, Y. Jia, F. Xia, R. Weihrich, F. Bachhuber and F. Pielnhofer, *Adv. Mater.*, 2015, **27**, 4423–4429.
28 J. P. Perdew, K. Burke and M. Ernzerhof, *Phys. Rev. Lett.*, 1996, **77**, 3865–3868.
29 G. Kresse and J. Furthmüller, *Phys. Rev. B: Condens. Matter*, 1996, **54**, 11169–11186.
30 J. Heyd, G. E. Scuseria and M. Ernzerhof, *J. Chem. Phys.*, 2003, **118**, 8207–8215.
31 A. Togo, F. Oba and I. Tanaka, *Phys. Rev. B: Condens. Matter*, 2008, **78**, 134106.
32 S. Nosé, *J. Chem. Phys.*, 1984, **81**, 511–519.
33 S. Grimme, *J. Comput. Chem.*, 2006, **27**, 1787–1799.
34 G. Wang, M. Si, A. Kumar and R. Pandey, *Appl. Phys. Lett.*, 2014, **104**, 213107.
35 C. D. Zeinalipour-Yazdi and C. Christofides, *J. Appl. Phys.*, 2009, **106**, 054318.
36 Q. Wei and X. Peng, *Appl. Phys. Lett.*, 2014, **104**, 251915.
37 G. Wang, G. C. Loh, R. Pandey and S. P. Karna, *Nanotechnol.*, 2016, **27**, 055701.
38 C. Lee, X. Wei, J. W. Kysar and J. Hone, *Science*, 2008, **321**, 385–388.
39 J. Qiao, X. Kong, Z.-X. Hu, F. Yang and W. Ji, *Nat. Commun.*, 2014, **5**, 4475.
40 X. Peng, Q. Wei and A. Copple, *Phys. Rev. B: Condens. Matter*, 2014, **90**, 085402.
41 J. Bardeen and W. Shockley, *Phys. Rev.*, 1950, **80**, 72.
42 S. Bruzzone and G. Fiori, *Appl. Phys. Lett.*, 2011, **99**, 222108.
43 B. Radisavljevic, A. Radenovic, J. Brivio, V. Giacometti and A. Kis, *Nat. Nanotechnol.*, 2011, **6**, 147–150.
44 P. E. Trevisanutto, C. Giorgetti, L. Reining, M. Ladisa and V. Olevano, *Phys. Rev. Lett.*, 2008, **101**, 226405.
45 D. Malko, C. Neiss, F. Viñes and A. Görling, *Phys. Rev. Lett.*, 2012, **108**, 086804.
46 Y. Yoon, K. Ganapathi and S. Salahuddin, *Nano Lett.*, 2011, **11**, 3768–3773.
47 Q. Yu, J. Lian, S. Siriponglert, H. Li, Y. P. Chen and S.-S. Pei, *Appl. Phys. Lett.*, 2008, **93**, 113103.
48 A. Reina, X. Jia, J. Ho, D. Nezich, H. Son, V. Bulovic, M. S. Dresselhaus and J. Kong, *Nano Lett.*, 2008, **9**, 30–35.
49 P. Vogt, P. De Padova, C. Quaresima, J. Avila, E. Frantzeskakis, M. C. Asensio, A. Resta, B. Ealet and G. Le Lay, *Phys. Rev. Lett.*, 2012, **108**, 155501.
50 C.-L. Lin, R. Arafune, K. Kawahara, N. Tsukahara, E. Minamitani, Y. Kim, N. Takagi and M. Kawai, *Appl. Phys. Express*, 2012, **5**, 045802.
51 Y. Lu, W. Xu, M. Zeng, G. Yao, L. Shen, M. Yang, Z. Luo, F. Pan, K. Wu and T. Das, *Nano Lett.*, 2014, **15**, 80–87.
52 S. Scott, M. Kral and S. Brown, *Surf. Sci.*, 2005, **587**, 175–184.
53 J. Sun, G. Zheng, H.-W. Lee, N. Liu, H. Wang, H. Yao, W. Yang and Y. Cui, *Nano Lett.*, 2014, **14**, 4573–4580.